THE JOURNAL OF PHYSICAL CHEMISTRY C

Article

pubs.acs.org/JPCC

Proton Hopping Mechanisms in a Protic Organic Ionic Plastic Crystal

Anirban Mondal and Sundaram Balasubramanian*

Chemistry and Physics of Materials Unit, Jawaharlal Nehru Centre for Advanced Scientific Research, Bangalore 560 064, India

Supporting Information

ABSTRACT: We elucidate the dynamics and mechanism of proton transport in a protic organic ionic plastic crystal (POIPC) [TAZ][pfBu] by means of Born−Oppenheimer molecular dynamics simulations at 400 K and zero humidity. The arrangement of ionic species in the crystal offers a two-dimensional hydrogen bond network along which an acidic proton can travel from one cation to another through a sequence of molecular reorientations. The results suggest spontaneous autodissociation of the N−H_N bond in the cation and multiple proton shuttle events from the cation's nitrogen to the anion's oxygen site in a native crystal. A complete proton transfer event is observed in simulations of a defective crystal with a single proton hole created in the cation. The barrier for proton transfer is determined using *ab initio* metadynamics simulations to be 7 kcal/mol, in agreement with experimental conductivity data. Using gas phase quantum chemical calculations, we propose [TAZ][$CF_3CF_2CH_2CF_2SO_3$] as a compound that can show enhanced conductivity compared to that of [TAZ][pfBu].

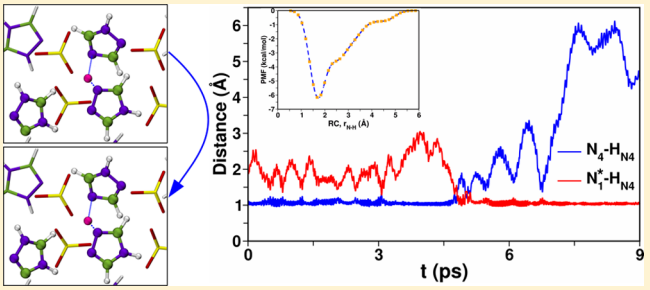

1. INTRODUCTION

Proton transfers and the consequent formation of protonic defects can lead to long-range proton conduction, a key process in the function of polymer electrolyte membrane fuel cells (PEMFCs).[1,2] PEMFCs are attractive electrochemical devices for use in transportation and portable power sources.[3,4] A critical component of PEMFCs is the electrolyte, which is a proton conductor. Often, a hydrated polymer electrolyte membrane is utilized to serve as the proton-conducting material in a PEMFC, and thus, it introduces a serious limitation in the operating temperature range of the cell because of the boiling point of water.[5,6]

In this regard, attempts have been made to develop water-free electrolyte materials that exhibit facile proton transport, e.g., imidazole in both solid and liquid phases,[7−10] imidazole derivatives,[6,11,12] proton-conducting functionalized polymers,[13−24] etc. Recently, a long-range proton transport phenomenon was also observed in framework materials consisting of suitable proton donor/acceptor sites, even at very low water concentrations.[25−27] Significant effort has also been focused on designing molecular crystals consisting of a hydrogen-bonded network that can act as water-free proton conductors.[28] However, it has been shown that systems with perfectly crystalline domains are not always conducive to proton transport[29,30] and that the contribution of residual water molecules in the conduction process is non-negligible.[21,31]

Organic ionic plastic crystals (OIPCs) composed of rotationally disordered mobile ions have emerged as solid-state ion conductors.[32−34] Although OIPCs have many positive attributes,[35,36] inherently they are aprotic in nature and are therefore not proton conductors. In this regard, protic OIPCs (POIPCs) are promising solid-state proton conductors for fuel cell applications.[33,37,38] Recently, Luo et al.[38] explored a 1,2,4-triazolium perfluorobutanesulfonate ([TAZ][pfBu]) POIPC, a novel electrolyte exhibiting attractive features, such as intrinsic anhydrous proton conductivity and a wide plastic crystal phase (360−450 K). Their studies of the [TAZ][pfBu] POIPC revealed high protonic conductivity in its plastic phase. In our previous work,[39] we studied the thermal phase behavior of [TAZ][pfBu] and its ion transport mechanism in its perfect crystalline form and in one with an ion pair vacancy via classical molecular dynamics simulations. However, proton diffusion, being a vital component of electrical conductivity in this system, was not considered because of the lack of bond breaking and re-forming capabilities in the simulation. This work focuses on understanding the microscopic proton conduction mechanism in [TAZ][pfBu] under anhydrous conditions by means of *ab initio* molecular dynamics simulations. Proton shuttling between ion neighbors was observed on a significant number of occasions in the native crystal, whereas complete proton transfer was seen only in simulations of a defective crystal with a single proton hole created in the cation. These observations delineate a long-range proton conduction path in the plastic crystalline phase of this POIPC. Gas phase quantum chemical calculations of novel variants of the anion suggest the possibility of a decreased barrier for proton transfer that can lead to enhanced electrical conductivities.

Received: August 16, 2016
Revised: September 22, 2016
Published: September 22, 2016

DOI: 10.1021/acs.jpcc.6b08274
J. Phys. Chem. C 2016, 120, 22903−22909

2. COMPUTATIONAL DETAILS

To understand the mechanism of proton transport in the plastic crystalline phase of the [TAZ][pfBu] POIPC (375−430 K as revealed by the experiments of Luo et al.[38]), the simulation temperature was set to 400 K. To obtain a pre-equilibrated configuration at 400 K, we first performed classical molecular dynamics (MD) simulations using the LAMMPS program package.[40] Details about the force field parameters and protocols are described elsewhere.[39] The initial configuration for the classical MD run was taken from the experimentally determined crystal structure[38] and contained 3 × 2 × 1 unit cells, with 624 atoms. The energy-minimized geometry was warmed to 400 K at a heating rate of 1 K per 100 ps in the fully flexible isothermal−isobaric (*NPT*) ensemble. A further equilibration of 5 ns was conducted in the *NVT* ensemble. A time step of 0.5 fs was used to integrate the equations of motion. The atom labeling scheme used in this work is presented in Figure 1.

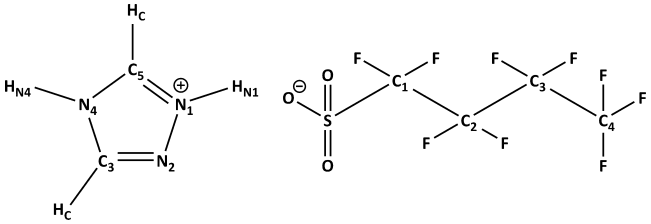

Figure 1. Atom labeling in [TAZ][pfBu] used throughout this article.

An equilibrated supercell from the classical MD trajectory was used to set up Born−Oppenheimer MD simulations with the electronic structure code CP2K,[41] using the Quickstep module.[42] The electronic structure was computed on the level of Kohn−Sham density functional theory,[43,44] utilizing the PBE exchange correlation functional,[45] with empirical dispersion correction (D3) from Grimme.[46] All valence electrons were treated with triple-ζ polarized basis sets with an energy cutoff of 280 Ry. Goedecker−Teter−Hutter (GTH)[47,48] pseudopotentials were applied to consider the effect of nuclei and core electrons. The time step to integrate the equations of motion was 0.4 fs. The system was equilibrated for 2 ps, which was followed by a production run for 60 ps in the canonical ensemble (*NVT*), with the temperature being maintained at 400 K using a Nosé−Hoover chain thermostat[49−51] with a coupling constant of 500 fs. The hydrogen bond network in the [TAZ][pfBu] POIPC is shown in Figure S1.

Biased MD simulations were performed on the POIPC to calculate the free energy profile for the transfer of the acidic hydrogen of the [TAZ$^+$] cation to the [pfBu$^-$] anion (see Figure S2). These were performed using the metadynamics method,[52] starting from configurations obtained from the equilibrium simulation described above. PLUMED version 2.0.1 patched with CP2K version 2.5.1 was employed to perform these metadynamics simulations.[53,54] The distance between the sulfonate oxygen (O) and the acidic hydrogen (either H_{N1} or H_{N4}) (hydrogen-bonded pair) was chosen to be the reaction coordinate (RC, r_{O-H}) to calculate the potential of mean force (PMF). Each of these runs was performed for a duration of 8 ps. An initial bias potential of 0.05 kcal/mol was utilized. The sum_hills program[53] was used to compute the PMF along the reaction coordinate.

3. RESULTS AND DISCUSSION

3.1. Structural Aspects. Radial distribution functions (RDFs) for the most relevant atom pairs (H_N−O and H_C−O) characterizing the properties of the hydrogen bond network in [TAZ][pfBu] are shown in Figure S3. C−H···O hydrogen bonding interactions are distinctively weaker than N−H···O hydrogen bonds. The hydrogen bond geometry between different atom pairs was further analyzed via combined probability distribution functions, and the same are shown in Figure S4. It is evident from Figure S4 that the sulfonate oxygens form more linear and, thus, stronger hydrogen bonds with the acidic hydrogen (H_N) atoms rather than with the H_C atoms. The stronger hydrogen bonds usually result in much lower barriers for proton transfer,[11] which can explain the facile intermolecular proton transfer events from the [TAZ$^+$] cation to the [pfBu$^-$] anion.

The change in the geometry of species during proton transfer events was studied by calculating the instantaneous N−H_N and O−H_N distances and the N−H_N···O angle, as shown in Figure 2. Throughout the course of equilibrium simulation, there were

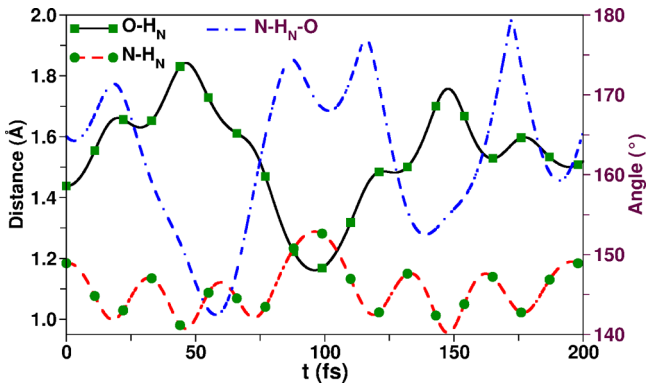

Figure 2. N−H_N and O−H_N distances and N−H_N···O angles during a proton transfer attempt event (around t = 100 fs in this trajectory) in the [TAZ][pfBu] POIPC. A few more such events along with a schematic depicting this angle and distances are shown in Figure S5.

instances in which the acidic protons were found to shuttle between the cation's nitrogen and the anion's oxygen. Figure 2 shows the interatomic distances during one such event (randomly chosen). In the figure, the covalent (∼1.0 Å) and hydrogen bond (∼1.8 Å) distances clearly show opposite behaviors at the 100 fs time point. At the crossing point, the intermolecular angle also becomes more linear to facilitate the transfer process. However, the heavy atom distances (N−O distance) in these simulations are not much different; the distances varied in the range of 2.45−2.47 Å.

3.2. Ion Rotation. There are three hydrogen bond acceptor sites (three oxygens) on the anion and two acidic hydrogens on the cation. The libration of cations allows the breaking and reformation of hydrogen bonds,[38,39] and thus, in principle, every oxygen atom of an anion can hydrogen bond with a neighboring cation; i.e., it can participate in the proton transfer process. However, during the duration of the simulation, only a fraction of anion oxygens attempt to acquire a proton from the cation. We have calculated the S−O bond distance for oxygen atoms that participate in a proton transfer event and those that do not. The distribution of such distances is shown in Figure S6. A clear distinction in sulfur−oxygen bond distance in two different instances is observed. The S−O bond distances for

DOI: 10.1021/acs.jpcc.6b08274
J. Phys. Chem. C 2016, 120, 22903−22909

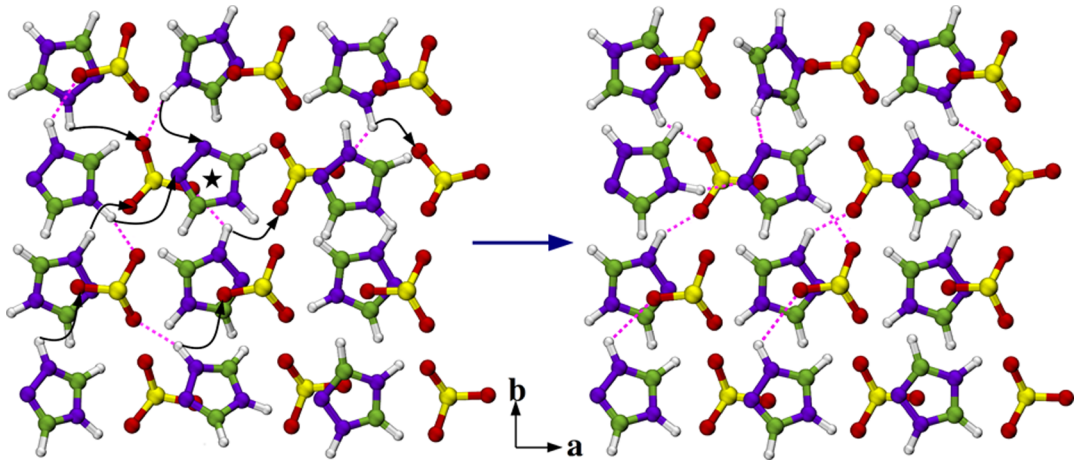

Figure 3. Structure of the defect crystal with the H_{N1} proton hole: before optimization (left) and after optimization (right). Only a part of the whole system has been shown, and alkyl tails are not shown for the sake of clarity. Color scheme: nitrogen, violet; carbon, green; hydrogen, white; oxygen, red; sulfur, yellow. Only those hydrogen bonds that take part in breakage and re-formation due to geometry optimization are shown. Other hydrogen bonds are intact and are not shown. Formation of a new hydrogen bond is shown with a curved arrow. The star denotes the activated cation.

sulfonate groups in which one of the oxygen atoms participates in a proton transfer attempt event (such as that depicted in Figure 2) are shorter than those whose oxygens do not participate in such events in the entire simulation trajectory. When an oxygen atom takes up a proton, the specific S−O bond distance becomes stretched, making the other two S−O bonds (in the same sulfonate group) contract. Thus, further examination of the role of the $-SO_3$ group in the proton transport mechanism is vital.

The rotational dynamics of the cation and of the $-SO_3$ group are presented in Figure S7. At short times, the correlation functions decay sharply; that for the cation rotation is faster than that for the $-SO_3$ group. Thus, it is possible that a $-SO_3$ group can participate as a mediator in the proton conduction process occurring along the hydrogen bond network in the crystallographic *a*−*b* plane (see Figure S8), also suggested by Luo et al. from experimental observations.[38] This process is further facilitated by the smaller rotational barrier (6.78 kcal/mol) of triazolium cations.[39] To improve our understanding of this plausible mechanism, we have calculated the distribution of residence times of acidic protons that are present within the covalent bond distance of the oxygen atoms of the $-SO_3$ group (see Figure S9). From the mean value of this distribution, it is evident that the H_N protons stay in the proximity of the $-SO_3$ oxygens (within 1.1 Å) for only 70−80 fs. Moreover, the time constant for the $-SO_3$ group rotational time correlation function was found to be around 250 fs (obtained from classical MD simulation of [TAZ][pfBu] performed at 400 K in our previous work).[39] Thus, before a $-SO_3$ group can transfer a proton to another cation, the same proton hops back to its original cation. This phenomenon can be rationalized in terms of the strong ionic environment in the crystal that restricts the formation of such neutral moieties. Such events may be plausible in a real system because of the presence of a finite number of defects. However, our simulations do not consider any such defects.

3.3. Defect Crystal Simulations. In an earlier work, Eikerling et al. demonstrated the relevance of defects to proton transport in a triflic acid monohydrate solid using *ab initio* MD simulations.[55] Their simulations revealed the formation of a stable Zundel ion ($H_5O_2^+$) in the defective crystal, followed by simultaneous rearrangement of neighboring $CF_3SO_3^-$ ions. They concluded that the intermediate state, i.e., the Zundel ion, functions as a mediator of proton transfer. In much the same spirit, we introduced a proton hole defect into the equilibrated native crystal by removing a proton from one of the triazolium cations, resulting in a net charge of the system of −1.0e. Proton holes in the cation were individually created by considering both acidic hydrogen atoms, i.e., H_{N1} and H_{N4} (see Figure 1). Three independent simulations in each of which a H_{N1} atom was removed were performed. The same was done with respect to the H_{N4} atom, as well. These six initial configurations were geometry-optimized at the same level of theory as in BOMD simulations of the native crystal. The gradients on the wave functions and on the nuclear positions were optimized with convergence criteria of 10^{-6} and 10^{-4} au, respectively. Two such quenched geometries (one from each set) were selected and were further employed for BOMD simulations at 400 K. After an initial equilibration for 1 ps, an analysis trajectory for 9 ps was generated.

3.4. Geometry Optimization of a Defective Crystal with One Proton Hole. The defective crystals (with one H_{N1} proton hole) before and after geometry optimization are shown in Figure 3. In the following, the cation in which the proton hole was created is termed the "activated cation". Prior to geometry optimization, both the N_1 and N_2 sites in an activated cation are chemically equivalent and are capable of accepting protons from neighboring cations (left panel of Figure 3). After optimization (right panel of Figure 3), both N_1 and N_2 sites of the activated cation are found to form a strong hydrogen bond with H_{N4} of another [TAZ^+] cation. In the case of the N_2 site, the donor [TAZ^+] cation is located in the same layer (crystallographic *a*−*b* plane) of the activated cation, while for the N_1 site, it was from a different layer. The initial and final distances between the N_1 and H_{N4} atoms were 3.83 and 1.89 Å, respectively, while the same for N_2 and H_{N4} were 3.01 and 1.73 Å, respectively. As a consequence of this rearrangement due to facile rotation of the triazolium cation, there were instances of breaking of the existing hydrogen bond and subsequent formation of new hydrogen bonds. This phenomenon can be rationalized in terms of local charge imbalance around the $-SO_3$ group created by the proton hole. When a [TAZ^+] cation rotates to act as a donor for a newly formed N_4−H···$N_{1/2}$ hydrogen bond, its existing hydrogen bond with a $-SO_3$ group is broken, and thus, the $-SO_3$ group is short one hydrogen bond,

DOI: 10.1021/acs.jpcc.6b08274
J. Phys. Chem. C 2016, 120, 22903−22909

i.e., slightly more electron rich than the other anions. As a result, breakage and formation of hydrogen bonds propagate in the whole system, and the same is depicted in Figure 3. Similar observations were made in the case of the H_{N4} proton hole system and are shown in Figure S10. This phenomenon has been observed in simulations started from all the six different initial configurations. The hydrogen bond network has been reconfigured, although no proton transfer takes place after geometry optimization.

3.5. BOMD Simulations of the Defective Crystal with One Proton Hole. Figure 4 displays interatomic distances

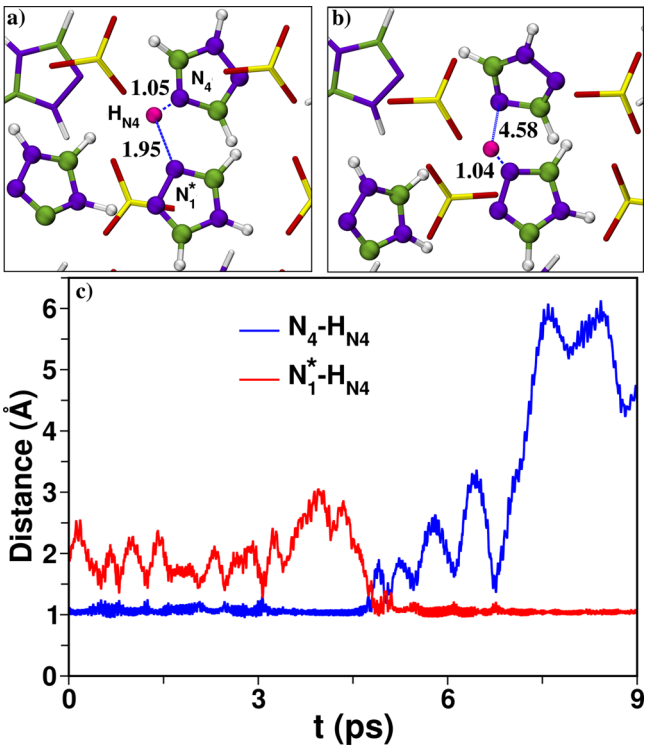

Figure 4. (a) Initial and (b) final snapshots of a small part of the simulation cell where the proton transfer event takes place. (c) Interatomic distances during the BOMD simulation of the defect crystal with the H_{N1} proton hole. Here, N_1* and N_4 sites belong to the activated cation and a normal cation from another layer, respectively.

during a proton exchange between triazolium cations from BOMD simulations of a defective crystal (H_{N1} proton hole). Within 5 ps of the trajectory, the H_{N4} atom of a neighboring cation that is located in another layer of the activated cation was found to be completely transferred to the N_1 site of the activated cation. During this period, the distance between the N_2 site of the activated cation and the H_{N4} hydrogen of a cation from the same layer increased by a significant amount. The proton was found to be covalently attached to the N_1 site of the activated cation for >4 ps. These observations suggest that intrinsic proton defects present in the plastic crystal can facilitate sequential proton conduction.

Simulations in which the H_{N4} atom was covalently (manually) attached to the -SO_3 group to which it was H-bonded in the native crystal were also conducted. After this addition, geometry optimization resulted in the restoration of the native crystal. However, addition of the same H^+ to a sulfonate group that is far from the activated cation followed by quenching and a BOMD simulation at 400 K produced a similar kind of proton shuttling as was observed in a native crystal.

3.6. *Ab Initio* Metadynamics Simulations. To characterize the energetics of proton transfer in this POIPC, we have performed *ab initio* metadynamics simulations along the proton transfer path. The free energy profiles obtained from three different runs were averaged and are presented in Figure 5. A

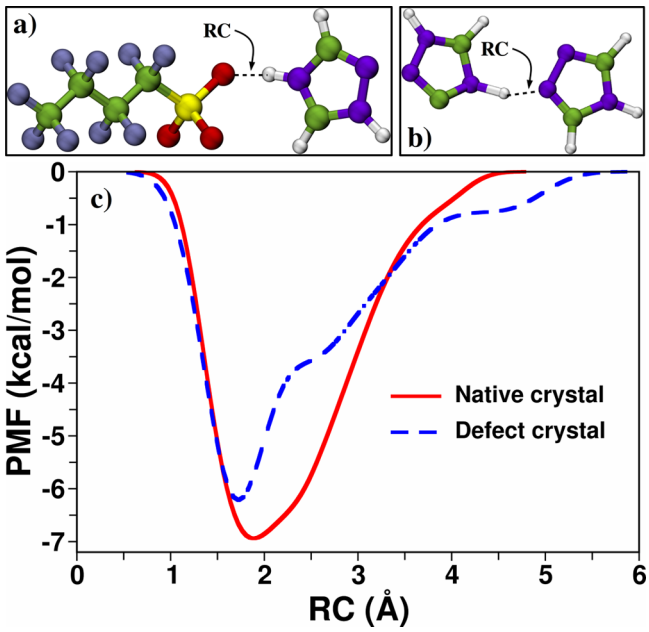

Figure 5. Reaction coordinates for proton transfer events in the (a) native crystal and (b) defect crystal with a single proton hole. (c) Free energy profile along the proton transfer coordinate in the plastic crystal phase of the [TAZ][pfBu] POIPC at 400 K.

minimum in the free energy profile was observed around 1.8 Å, which is the typical hydrogen bond distance between the acidic proton and the sulfonate oxygen. The free energy barrier for dissociation of the proton from the sulfonate oxygen is around 7.0 kcal/mol. Thus, the system with the protonated [TAZ^+] cation and [$pfBu^-$] anion is more stable than a pair of neutral species by ~7 kcal/mol. Note that both states are located in a matrix of ions in the crystalline environment, which obviously would prefer that the two molecular species be ionic rather than neutral. Experimental ionic conductivity data[38] for this POIPC in the plastic crystal region (373−430 K) show an activation energy barrier of 8.8 kcal/mol. In addition, the measured experimental conductivity was reported to be mainly protonic in nature.[38] It is thus evident that the calculated free energy barrier for the proton transfer process is in good agreement with experimental activation energy. For the sake of comparison, we have performed a similar calculation in which the distance between the sulfonate oxygen (O) and the acidic hydrogen (H_{N1}) (hydrogen-bonded pair) was chosen as the reaction coordinate. The free energy profile was quite similar to that shown in Figure 5, and the free energy barrier was around 7.5 kcal/mol.

Furthermore, the free energy barrier for proton transfer in a defective crystal (H_{N1} proton hole) was determined in a fashion similar to that described above. The distance between the N_1 site of the activated cation and the H_{N4} atom of a cation from the same layer (hydrogen-bonded pair) was chosen as the

DOI: 10.1021/acs.jpcc.6b08274
J. Phys. Chem. C 2016, 120, 22903−22909

reaction coordinate. The free energy profile is displayed in Figure 5, and the barrier was around 6.2 kcal/mol.

3.7. Gas Phase Calculations. To substantiate the energetics of proton transfer in [TAZ][pfBu], we have performed gas phase calculations using an ion pair in Gaussian 09.[56] Starting configurations were constructed using the GaussView package.[57] Geometry optimization was performed at the M06/aug-cc-pVDZ level of theory. Frequency analysis within the harmonic approximation was conducted to confirm that the optimized geometry is a minimum. In addition, the transition state was validated by performing intrinsic reaction coordinate (IRC) calculations that could allow the transition state to be connected to both the reactant and the product. The energy barrier obtained from IRC calculation (see Figure 6)

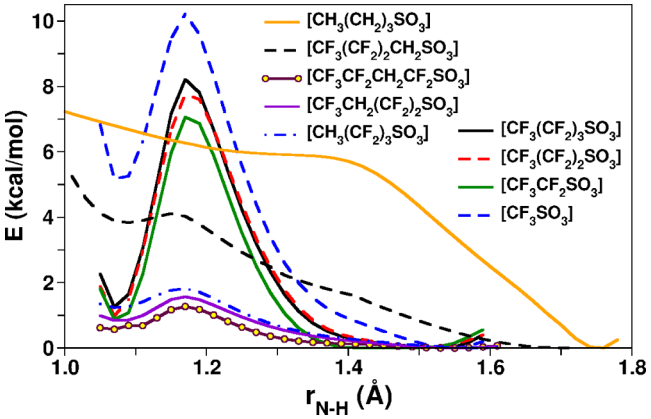

Figure 6. Energy barrier associated with the proton transfer reaction obtained from gas phase calculations at the M06/aug-cc-pVDZ level of theory. The common cation is [TAZ^+].

was 6.8 kcal/mol, which is in good agreement with the free energy barrier obtained from *ab initio* metadynamics simulations. IRC calculation was also performed considering proton transfer from the N_4 site to the sulfonate oxygen, and the energy barrier was found to be around 6.5 kcal/mol. Thus, the transfer of either of the acidic protons to the anion is equally probable, consistent with results obtained from *ab initio* metadynamics simulations.

Gas phase calculations on an ion pair (see Figure 6) show that the neutral species is stable over the ionic one by just 1.1 kcal/mol, but the crystalline form is stabilized by multiple hydrogen bond networks and long-range electrostatic interactions, which are absent in the gas phase calculation. At this point, we are interested in exploring ways to decrease the energy barrier for proton transfer in the POIPC (which could enhance proton conduction) without altering the plastic crystallinity much. For this purpose, we adopted two simple procedures to increase the anion basicity: (i) reduction of the alkyl tail length in the anion and (ii) partial substitution of fluorine atoms on different carbons in the anion with hydrogens. IRC calculations on several ion pairs have been performed following the same protocol that is discussed above. It is to be noted that absolute values of proton transfer barriers may change in a PCM model; however, the relative energy barriers would provide the same trend (which is the quantity of interest here) as reported in the current gas phase calculations. The barrier for proton transfer decreased from a value of 6.8 to 5.1 kcal/mol with a change from the [$pfBu^-$] anion to [$CF_3SO_3^-$] (see Figure 6). In this process, the van der Waals interaction between the alkyl tails may be compromised by a large amount, which in turn can destabilize the crystal and/or reduce the temperature range of the plastic crystal phase. On the other hand, either the complete or partial substitution at the C_1 site of the fluorine atoms with hydrogens resulted in a barrierless process (see Figure 6), which indicates that the ionic species is not stable compared to the neutral one. However, substitution at other carbon sites, e.g., C_2, C_3, or C_4, produced reasonable profiles that balanced both the energy barrier and the stability of the ionic state. Considering all the profiles obtained from IRC calculations, an anion with a perfluorobutyl tail in which the fluorine atoms at the C_2 position alone are substituted with hydrogens yields a low barrier (0.6 kcal/mol) for proton transfer and will likely not affect the crystal stability much. Thus, we believe the [TAZ][$CF_3CF_2CH_2CF_2SO_3$] POIPC could be a promising candidate for high proton conductivity with a wide plastic crystal phase as compared to that of [TAZ][pfBu].

4. CONCLUSIONS

The details of proton transport in the plastic crystalline phase of the [TAZ][pfBu] POIPC have been investigated using Born−Oppenheimer molecular dynamics simulations. The ions pack in layers perpendicular to the crystallographic *c* axis, and this results in the formation of a hydrogen bond network along the crystallographic *a*−*b* plane (see Figure S1). *Ab initio* molecular dynamics simulations detect spontaneous autodissociation of the acidic proton (H_N), in the absence of any water molecule. No significant conduction of a proton along the hydrogen bond network was seen, and the back transfer of a proton from the anion back to the cation always occurred in tens of femtoseconds in the native crystal. The rotational correlations for both the cation and the -SO_3 group decay sharply at short times, which suggests the importance of molecular reorientation in the proton transport process.

However, complete proton transfers were observed in simulations of a defective crystal in which one proton hole was created by removing one of the acidic protons in a triazolium cation. The optimized structure demonstrated the formation of a strong hydrogen bond between the N_1 and N_2 sites of the "activated cation" and H_{N4} of another cation.

The energy barrier for proton transfer was determined by free energy calculations, and the estimated barrier was found to be around 7.0 kcal/mol against the experimentally determined activation barrier of 8.77 kcal/mol obtained from conductivity measurements.[38] The current simulations treat the proton as a classical particle. However, nuclear quantum effects can affect the barrier for its transfer and need to be taken into account. This is beyond the scope of this work. Gas phase IRC calculations on ion pairs suggest [TAZ][$CF_3CF_2CH_2CF_2SO_3$] to be a promising material for a proton-conducting membrane. These observations illustrate that high-temperature dry fuel cell membrane materials are not very far from our reach, and they would remarkably enhance the efficiency of all hydrogen full cell systems.

■ ASSOCIATED CONTENT

Supporting Information

The Supporting Information is available free of charge on the ACS Publications website at DOI: 10.1021/acs.jpcc.6b08274.

Hydrogen bond network, reaction coordinate for free energy calculations, RDFs, CDFs, S−O bond distribu-

DOI: 10.1021/acs.jpcc.6b08274
J. Phys. Chem. C 2016, 120, 22903−22909

tion, rotational correlation functions, and hydrogen bond time correlation functions (PDF)

AUTHOR INFORMATION

Corresponding Author

*E-mail: bala@jncasr.ac.in. Phone: +91 (80) 2208 2808. Fax: +91 (80) 2208 2766.

Notes

The authors declare no competing financial interest.

ACKNOWLEDGMENTS

A.M. thanks Anurag Prakash Sunda for helpful discussions. We thank DST for support.

REFERENCES

(1) Kreuer, K.-D. Proton Conductivity: Materials and Applications. *Chem. Mater.* **1996**, *8*, 610−641.

(2) Kreuer, K.-D.; Paddison, S. J.; Spohr, E.; Schuster, M. Transport in Proton Conductors for Fuel-Cell Applications: Simulations, Elementary Reactions, and Phenomenology. *Chem. Rev.* **2004**, *104*, 4637−4678.

(3) Gasteiger, H. A.; Marković, N. M. Just a Dream−or Future Reality? *Science* **2009**, *324*, 48−49.

(4) Debe, M. K. Electrocatalyst Approaches and Challenges for Automotive Fuel Cells. *Nature* **2012**, *486*, 43−51.

(5) Nimmanpipug, P.; Laosombat, T.; Sanghiran Lee, V.; Vannarat, S.; Chirachanchai, S.; Yana, J.; Tashiro, K. Proton Transfer Mechanism of 1,3,5-tri(2-benzimidazolyl) Benzene with a Unique Triple-stranded Hydrogen Bond Network as Studied by DFT-MD Simulations. *Chem. Eng. Sci.* **2015**, *137*, 404−411.

(6) Eisbein, E.; Joswig, J.-O.; Seifert, G. Enhanced Proton-transfer Activity in Imidazole@MIL-53(Al) Systems Revealed by Molecular-dynamics Simulations. *Microporous Mesoporous Mater.* **2015**, *216*, 36−41.

(7) Iannuzzi, M. Proton Transfer in Imidazole-based Molecular Crystals. *J. Chem. Phys.* **2006**, *124*, 204710.

(8) Münch, W.; Kreuer, K.-D.; Silvestri, W.; Maier, J.; Seifert, G. The Diffusion Mechanism of an Excess Proton in Imidazole Molecule Chains: First Results of An Ab Initio Molecular Dynamics Study. *Solid State Ionics* **2001**, *145*, 437−443.

(9) Chen, H.; Yan, T.; Voth, G. A. A Computer Simulation Model for Proton Transport in Liquid Imidazole. *J. Phys. Chem. A* **2009**, *113*, 4507−4517.

(10) Li, A.; Cao, Z.; Li, Y.; Yan, T.; Shen, P. Structure and Dynamics of Proton Transfer in Liquid Imidazole. A Molecular Dynamics Simulation. *J. Phys. Chem. B* **2012**, *116*, 12793−12800.

(11) Vilčiauskas, L.; Tuckerman, M. E.; Melchior, J. P.; Bester, G.; Kreuer, K.-D. First Principles Molecular Dynamics Study of Proton Dynamics and Transport in Phosphoric Acid/Imidazole (2:1) System. *Solid State Ionics* **2013**, *252*, 34−39.

(12) Thisuwan, J.; Sagarik, K. Proton Dissociation and Transfer in a Phosphoric Acid Doped Imidazole System. *RSC Adv.* **2014**, *4*, 61992−62008.

(13) Roy, S.; Ataol, T. M.; Müller-Plathe, F. Molecular Dynamics Simulations of Heptyl Phosphonic Acid: A Potential Polymer Component for Fuel Cell Polymer Membrane. *J. Phys. Chem. B* **2008**, *112*, 7403−7409.

(14) Schuster, M.; Rager, T.; Noda, A.; Kreuer, K. D.; Maier, J. About the Choice of the Protogenic Group in PEM Separator Materials for Intermediate Temperature, Low Humidity Operation: A Critical Comparison of Sulfonic Acid, Phosphonic Acid and Imidazole Functionalized Model Compounds. *Fuel Cells* **2005**, *5*, 355−365.

(15) Joswig, J.-O.; Seifert, G. Aspects of the Proton Transfer in Liquid Phosphonic Acid. *J. Phys. Chem. B* **2009**, *113*, 8475−8480.

(16) Vilciauskas, L.; Paddison, S. J.; Kreuer, K.-D. Ab Initio Modeling of Proton Transfer in Phosphoric Acid Clusters. *J. Phys. Chem. A* **2009**, *113*, 9193−9201.

(17) Vilčiauskas, L.; Tuckerman, M. E.; Bester, G.; Paddison, S. J.; Kreuer, K.-D. The Mechanism of Proton Conduction in Phosphoric Acid. *Nat. Chem.* **2012**, *4*, 461−466.

(18) Steininger, H.; Schuster, M.; Kreuer, K. D.; Kaltbeitzel, A.; Bingol, B.; Meyer, W. H.; Schauff, S.; Brunklaus, G.; Maier, J.; Spiess, H. W. Intermediate Temperature Proton Conductors for PEM Fuel Cells Based on Phosphonic Acid as Protogenic Group: A Progress Report. *Phys. Chem. Chem. Phys.* **2007**, *9*, 1764−1773.

(19) Kreuer, K.-D.; Wohlfarth, A. Limits of Proton Conductivity. *Angew. Chem., Int. Ed.* **2012**, *51*, 10454−10456.

(20) Vuilleumier, R.; Borgis, D. Proton Conduction: Hopping Along Hydrogen Bonds. *Nat. Chem.* **2012**, *4*, 432−433.

(21) Ludueña, G. A.; Kühne, T. D.; Sebastiani, D. Mixed Grotthuss and Vehicle Transport Mechanism in Proton Conducting Polymers from Ab initio Molecular Dynamics Simulations. *Chem. Mater.* **2011**, *23*, 1424−1429.

(22) Kabbe, G.; Wehmeyer, C.; Sebastiani, D. A Coupled Molecular Dynamics/Kinetic Monte Carlo Approach for Protonation Dynamics in Extended Systems. *J. Chem. Theory Comput.* **2014**, *10*, 4221−4228.

(23) Weber, J.; Kreuer, K.-D.; Maier, J.; Thomas, A. Proton Conductivity Enhancement by Nanostructural Control of Poly(benzimidazole)-Phosphoric Acid Adducts. *Adv. Mater.* **2008**, *20*, 2595−2598.

(24) Wehmeyer, C.; Schrader, M.; Andrienko, D.; Sebastiani, D. Water-Free Proton Conduction in Hexakis(p-Phosphonatophenyl)-benzene Nanochannels. *J. Phys. Chem. C* **2013**, *117*, 12366−12372.

(25) Umeyama, D.; Horike, S.; Inukai, M.; Itakura, T.; Kitagawa, S. Inherent Proton Conduction in a 2D Coordination Framework. *J. Am. Chem. Soc.* **2012**, *134*, 12780−12785.

(26) Pardo, E.; Train, C.; Gontard, G.; Boubekeur, K.; Fabelo, O.; Liu, H.; Dkhil, B.; Lloret, F.; Nakagawa, K.; Tokoro, H.; et al. High Proton Conduction in a Chiral Ferromagnetic Metal-Organic Quartz-like Framework. *J. Am. Chem. Soc.* **2011**, *133*, 15328−15331.

(27) Sadakiyo, M.; Ōkawa, H.; Shigematsu, A.; Ohba, M.; Yamada, T.; Kitagawa, H. Promotion of Low-Humidity Proton Conduction by Controlling Hydrophilicity in Layered Metal-Organic Frameworks. *J. Am. Chem. Soc.* **2012**, *134*, 5472−5475.

(28) Maly, K. E.; Gagnon, E.; Maris, T.; Wuest, J. D. Engineering Hydrogen-Bonded Molecular Crystals Built from Derivatives of Hexaphenylbenzene and Related Compounds. *J. Am. Chem. Soc.* **2007**, *129*, 4306−4322.

(29) Lee, Y. J.; Bingöl, B.; Murakhtina, T.; Sebastiani, D.; Meyer, W. H.; Wegner, G.; Spiess, H. W. High-Resolution Solid-State Studies NMR of Poly(vinyl phosphonic acid) Proton-Conducting Polymer: Molecular Structure and Proton Dynamics. *J. Phys. Chem. B* **2007**, *111*, 9711−9721.

(30) Lee, Y. J.; Murakhtina, T.; Sebastiani, D.; Spiess, H. W. ^{2}H Solid-State NMR of Mobile Protons: It Is Not Always the Simple Way. *J. Am. Chem. Soc.* **2007**, *129*, 12406−12407.

(31) Siwick, B. J.; Bakker, H. J. On the Role of Water in Intermolecular Proton-Transfer Reactions. *J. Am. Chem. Soc.* **2007**, *129*, 13412−13420.

(32) MacFarlane, D. R.; Forsyth, M. Plastic Crystal Electrolyte Materials: New Perspectives on Solid State Ionics. *Adv. Mater.* **2001**, *13*, 957−966.

(33) Pringle, J. M. Recent Progress in the Development and Use of Organic Ionic Plastic Crystal Electrolytes. *Phys. Chem. Chem. Phys.* **2013**, *15*, 1339−1351.

(34) Jin, L.; Nairn, K. M.; Forsyth, C. M.; Seeber, A. J.; MacFarlane, D. R.; Howlett, P. C.; Forsyth, M.; Pringle, J. M. Structure and Transport Properties of a Plastic Crystal Ion Conductor: Diethyl-(methyl) (isobutyl)phosphonium Hexafluorophosphate. *J. Am. Chem. Soc.* **2012**, *134*, 9688−9697.

(35) Armel, V.; Forsyth, M.; MacFarlane, D. R.; Pringle, J. M. Organic Ionic Plastic Crystal Electrolytes; a New Class of Electrolyte for High Efficiency Solid State Dye-sensitized Solar Cells. *Energy Environ. Sci.* **2011**, *4*, 2234−2239.

(36) Jin, L.; Howlett, P. C.; Pringle, J. M.; Janikowski, J.; Armand, M.; MacFarlane, D. R.; Forsyth, M. An Organic Ionic Plastic Crystal

DOI: 10.1021/acs.jpcc.6b08274
J. Phys. Chem. C 2016, 120, 22903−22909

Electrolyte for Rate Capability and Stability of Ambient Temperature Lithium Batteries. *Energy Environ. Sci.* **2014**, *7*, 3352−3361.
(37) Luo, J.; Conrad, O.; Vankelecom, I. F. J. Imidazolium Methanesulfonate as a High Temperature Proton Conductor. *J. Mater. Chem. A* **2013**, *1*, 2238−2247.
(38) Luo, J.; Jensen, A. H.; Brooks, N. R.; Sniekers, J.; Knipper, M.; Aili, D.; Li, Q.; Vanroy, B.; Wubbenhorst, M.; Yan, F.; et al. 1,2,4-Triazolium Perfluorobutanesulfonate as an Archetypal Pure Protic Organic Ionic Plastic Crystal Electrolyte for All-Solid-State Fuel Cells. *Energy Environ. Sci.* **2015**, *8*, 1276−1291.
(39) Mondal, A.; Sunda, A. P.; Balasubramanian, S. Thermal Phase Behavior and Ion Hopping in a 1,2,4-Triazolium Perfluorobutanesulfonate Protic Organic Ionic Plastic Crystal. *Phys. Chem. Chem. Phys.* **2016**, *18*, 2047−2053.
(40) Plimpton, S. Fast Parallel Algorithms for Short-Range Molecular Dynamics. *J. Comput. Phys.* **1995**, *117*, 1−19.
(41) Hutter, J.; Iannuzzi, M.; Schiffmann, F.; VandeVondele, J. CP2K: Atomistic Simulations of Condensed Matter Systems. *Wiley Interdiscip. Rev. Comput. Mol. Sci.* **2014**, *4*, 15−25.
(42) VandeVondele, J.; Krack, M.; Mohamed, F.; Parrinello, M.; Chassaing, T.; Hutter, J. Quickstep: Fast and Accurate Density Functional Calculations Using a Mixed Gaussian and Plane Waves Approach. *Comput. Phys. Commun.* **2005**, *167*, 103−128.
(43) Hohenberg, P.; Kohn, W. Inhomogeneous Electron Gas. *Phys. Rev.* **1964**, *136*, B864−B871.
(44) Kohn, W.; Sham, L. J. Self-Consistent Equations Including Exchange and Correlation Effects. *Phys. Rev.* **1965**, *140*, A1133−A1138.
(45) Perdew, J. P.; Burke, K.; Ernzerhof, M. Generalized Gradient Approximation Made Simple. *Phys. Rev. Lett.* **1996**, *77*, 3865−3868.
(46) Grimme, S.; Antony, J.; Ehrlich, S.; Krieg, H. A Consistent and Accurate Ab Initio Parametrization of Density Functional Dispersion Correction (DFT-D) for the 94 Elements H-Pu. *J. Chem. Phys.* **2010**, *132*, 154104.
(47) Goedecker, S.; Teter, M.; Hutter, J. Separable Dual-space Gaussian Pseudopotentials. *Phys. Rev. B: Condens. Matter Mater. Phys.* **1996**, *54*, 1703−1710.
(48) Hartwigsen, C.; Goedecker, S.; Hutter, J. Relativistic Separable Dual-space Gaussian Pseudopotentials from H to Rn. *Phys. Rev. B: Condens. Matter Mater. Phys.* **1998**, *58*, 3641−3662.
(49) Nosé, S. A Unified Formulation of the Constant Temperature Molecular Dynamics Methods. *J. Chem. Phys.* **1984**, *81*, 511−519.
(50) Nosé, S. A Molecular Dynamics Method for Simulations in the Canonical Ensemble. *Mol. Phys.* **1984**, *52*, 255−268.
(51) Martyna, G. J.; Klein, M. L.; Tuckerman, M. Nosé-Hoover Chains: The Canonical Ensemble via Continuous Dynamics. *J. Chem. Phys.* **1992**, *97*, 2635−2643.
(52) Laio, A.; Gervasio, F. L. Metadynamics: a Method to Simulate Rare Events and Reconstruct the Free Energy in Biophysics, Chemistry and Material Science. *Rep. Prog. Phys.* **2008**, *71*, 126601−126623.
(53) Bonomi, M.; Branduardi, D.; Bussi, G.; Camilloni, C.; Provasi, D.; Raiteri, P.; Donadio, D.; Marinelli, F.; Pietrucci, F.; Broglia, R. A.; et al. PLUMED: A Mortable Plugin for Free-energy Calculations with Molecular Dynamics. *Comput. Phys. Commun.* **2009**, *180*, 1961−1972.
(54) Tribello, G. A.; Bonomi, M.; Branduardi, D.; Camilloni, C.; Bussi, G. PLUMED 2: New Feathers for an Old Bird. *Comput. Phys. Commun.* **2014**, *185*, 604−613.
(55) Eikerling, M.; Paddison, S. J.; Pratt, L. R.; Zawodzinski, T. A., Jr. Defect Structure for Proton Transport in a Triflic Acid Monohydrate Solid. *Chem. Phys. Lett.* **2003**, *368*, 108−114.
(56) Frisch, M. J.; Trucks, G. W.; Schlegel, H. B.; Scuseria, G. E.; Robb, M. A.; Cheeseman, J. R.; Scalmani, G.; Barone, V.; Mennucci, B.; et al. *Gaussian 09*, revision D.01; Gaussian Inc.: Wallingford, CT, 2009.
(57) Dennington, R.; Keith, T.; Millam, J. *GaussView*, version 5; Semichem Inc.: Shawnee Mission, KS, 2009.

DOI: 10.1021/acs.jpcc.6b08274
J. Phys. Chem. C 2016, 120, 22903−22909